UMEO: Uranus Magnetosphere Exploration Orbiter

Team Green: J. Balan, M. Doležel, L.C. Francalanza, A. González Del Castillo, J. Grabowski, T. Grundnig, A. Hamieh, S. Holdcroft, M. Jurczak, P. Kourkoutas, A. Peschel, R. Savonet, J. Servin, C. Thomopoulos, U. Wasilewska
Tutors: F. Enengl, W. Jellema
22 July 2026

Abstract

Ice giants remain among the least explored bodies in the Solar System, even though they are our closest analogues to the most common class of exoplanets in the galaxy in terms of their size and their obliquity. Uranus is particularly unique because of its extreme axial tilt and off-centered magnetic field, however it is poorly studied. The Uranus Magnetosphere Exploration Orbiter (UMEO) is a mission concept designed to investigate the high-energy processes that shape this unique environment. Over 22 science orbits per year and 5 years of science, UMEO will characterise Uranus' magnetic and gravity fields, observe how the magnetosphere interacts with the solar wind, and investigate the structure and dynamics of its radiation belts and plasmoids. To achieve these objectives, UMEO is equipped with a payload of six instruments, primarily featuring a magnetometer, a plasma wave instrument, and a particle environment package. The UMEO orbiter has an estimated wet mass of 2240 kg and a dry mass of 849 kg. Power generation in the outer Solar System is provided by a GPHS-RTG, enabling sustained operations at Uranus. The spacecraft is planned for launch aboard an Ariane 64 launch vehicle in 2038, followed by a 14.2-year interplanetary cruise trajectory incorporating multiple Venus and Earth gravity assists. The total mission cost is estimated at 1363 M€, placing it within the cost cap of an ESA L-class mission.

keywords: Uranus, magnetosphere, magnetic reconnection, radiation belt, aurora, ion loss, Ariane 64

1. INTRODUCTION

Our understanding of exoplanetary magnetic fields and their atmospheric high-energy processes, which are crucial to planetary evolution, remains extremely limited due to exploration constraints. Since highly oblique planets are very common among exoplanets (Millholland et al., 2019), a mission to such an archetype would be particularly valuable. The Solar System is essential to filling this gap, as it is the only region where in-situ measurements are possible. As such, exploring Uranus, which still remains as an ice giant among the least studied planetary environments, would provide crucial observational constraints on magnetospheric and atmospheric processes (Fletcher et al., 2020). The most relevant current observations rely on the brief visit of Voyager 2 in 1986 (Stone et al., 1986). Consequently, in order to address this knowledge gap, investigating the Uranus' magnetosphere with an orbiter in greater depth allows to connect the further exploration of the Solar System with a knowledge gain in the exoplanetary context.

2. SCIENCE CASE

2.1. Magnetosphere and Internal Dynamo

The data collected during the Voyager 2 mission showed a highly anomalous and non-dipolar magnetic field, hinting to dynamo processes radically different than the ones observed in the closer planets (Connerney et al., 1987). Currently, there is no established hypothesis for this mechanism, with the possibilities varying from shallow depth dynamos in Uranus' outer shell to proton migration driven by thermoelectric effects in superionic water ice within the mantle (Liu et al., 2026; Stanley et al., 2004). Furthermore, subsequent studies have shown that the Voyager 2 encounter occurred during an unusually compressed magnetospheric state, meaning that our current understanding is based on observations obtained under atypical conditions (Jasinski et al., 2024). Therefore, solving the internal composition structure of the planet and mapping the magnetic field (Parisi et al., 2024) is essential for a in-depth understanding of the formation and internal processes of magnetosphere physics.

2.2. Magnetic Reconnection, Energy and Plasma Transport Processes

A magnetosphere does not represent a static environment, e.g. magnetic reconnection of plasma particles moving along opposite directed magnetic field lines alters the movement of the interplanetary plasma. On the one hand, planets such as Earth follow the solar-wind driven Dungey-cycle reconnection mechanism (Ma et al., 2017). On the other hand, Kelvin-Helmholtz instabilities due to the viscous characteristic of the interplanetary plasma can provoke efficient reconnection frequencies at the magnetopause as well (Ma et al., 2017). In case of Uranus, Masters, 2014 expected, based on the high distance to the Sun, the Dungey cycle and thus the reconnection rate at the magnetopause to be less prominent. Nevertheless, seasonal change and the magnetic field orientation might impact these two reconnection causes (Masters, 2014). A mission to Uranus would help unravel the dependence on the solar distance, obliquity and seasonality for the Dungey and Kelvin-Helmholtz cycle, in turn helping to understand reconnection of ice giants and for oblique exoplanets.

2.3. Aurorae and Upper Atmosphere Interactions

Magnetic reconnection accelerates charged particles along magnetic field lines toward the poles, where collisions with atmospheric gases generate auroral emission, primarily in the ultraviolet. Despite decades of observations, Uranus's aurorae remain poorly understood. Voyager 2 first detected a patchy aurora for Uranus (Herbert, 2009), while later Hubble observations revealed a similarly variable geometry (Lamy et al., 2012). More recent JWST data indicate a puzzling long-term cooling of the upper atmosphere to about 415 K, which is over 300 K colder than during the Voyager flyby, with no established explanation (Melin et al., 2025).

Aurorae trace how energetic particles enter Uranus's atmosphere, yet existing observations lack sufficient spatial and temporal coverage (Bhardwaj et al., 2000). Mapping them would reveal how dayside reconnection and Uranus's unusual magnetic geometry control atmospheric energy input (Paty et al., 2020; Turner et al., 2024), providing valuable constraints for exoplanetary upper-atmosphere and space-weather models (Fletcher et al., 2020).

2.4. Atmospheric Ion Loss Processes

Upper atmospheres experience ion loss through processes such as plasmaspheric outflow caused by magnetotail reconnection, the latter producing plasmoids, which are bundles of magnetic field containing planetary plasma that transport atmospheric material into interplanetary space (Gronoff et al., 2020; Treumann et al., 2001).

A re-analysis of the Voyager 2 flyby by DiBraccio et al. (2019) identified a cylindrical plasmoid (0.5–$3.3\, R_U \times 8$–$16\, R_U$) carrying an estimated atmospheric mass of approximately 430 ± 270 kg. Combined with evidence for dayside reconnection occurring on timescales of approximately 17 h (Richardson et al., 1988), this suggests that plasmoid ejection may represent a significant pathway for atmospheric ion loss at Uranus. Observations of H Lyα emission by the Hubble Space Telescope further support the possibility that atmospheric escape varies with season, particularly around equinox (Joshi et al., 2025).

However, because Voyager 2 intercepted only the edge of a single plasmoid during a brief flyby, its observations were insufficient to determine the frequency, a solid morphology or contribution of plasmoids to Uranus' long-term atmospheric escape (DiBraccio et al., 2019). Consequently, it remains unknown whether plasmoid-driven escape is an episodic process or the dominant mechanism governing atmospheric ion loss. Resolving this uncertainty is essential not only for understanding the evolution of Uranus's atmosphere but also for constraining atmospheric escape processes for common highly oblique, magnetised exoplanets (Millholland et al., 2019), for which Uranus provides the closest natural analogue.

2.5. Radiation Belt Mechanisms

The mission further aims to determine why Uranus was observed to have a radiation belt approaching the Kennel-Petschek limit in intensity, comparable to that of Jupiter, despite Uranus having a plasma source of two orders of magnitude weaker (Mauk et al., 2010; McNutt Jr. et al., 1987). This challenges the conventional view of planetary radiation belts, in which intense radiation belts are expected to require a substantial internal plasma source to supply particles for subsequent transport and acceleration (Mauk et al., 2010). For Uranus, Allen et al. (2025) proposed the hypothesis that the anomalously intense radiation belts are sustained through lower-band whistler-mode chorus waves, which accelerate CIR-injected seed electrons to relativistic energies.

Additionally, magnetospheric pre-conditioning may modify the seed electron population, thereby increasing the efficiency with which lower-band chorus waves accelerate particles to relativistic energies (Allen et al., 2025). Thus, confirming this mechanism would not only explain the origin of Uranus' unexpectedly intense radiation belts, but would also establish whether wave-driven particle acceleration represents a fundamental process governing radiation belt formation across diverse magnetospheres as many of the exoplanets discovered to date are thought to resemble Uranus (Millholland et al., 2019).

3. MISSION GOALS

The Uranus Magnetosphere Exploration Orbiter Mission (UMEO) will set out to further our understanding of the mechanisms behind the origin, structure and dynamics of magnetospheres and characterise the fundamental physics that govern the related scientific phenomenons of magnetic reconnection, aurora, atmospheric ion loss processes and radiation belts.

3.1. Science Questions and Objectives

The mission will therefore attempt to address the fundamental scientific questions (SQ) specifically, by fulfilling the outlined scientific objectives (SO) which are demonstrated in Table 1.

3.2. Science Requirements

Table 1 outlines the physical quantities and the ranges required for the scientific objectives, and the instruments identified as capable of making these measurements.
The minimum science required :

1. The gravity measurement requires 8-10 close passes in a distance $\leq 1.1\ R_U$ or ≤ 25000 km from the atmosphere (Parisi et al., 2024) and the magnetosphere measurements requires $\sim$20 close passes in 2-4 years at 1000-5000 km from the surface (Simon et al., 2021).
2. The plasma characterization requires 8x2 min measurements at both sides of the magnetopause crossing for 3 years, as well as continuously for the solar wind upstream and ion/electron energy spectra in the outside bow shock (Sibeck et al., 2022).
3. All measurements for the aurorae are done once every 5 orbits in the polar regions distributed over a minimum of $\sim$4 years, in order to study different magnetic configurations and solar wind conditions (Lamy, 2020).
4. Observations need to be executed in the magnetotail for at least 5 years (assuming this time period could be extrapolated to represent the solar cycle), in order to obtain the plasmoid occurrence depending on the solar wind.
5. Ideally the full length of the mission is needed to determine the time variability of radiation belts. A minimum of 1 year in orbit is sufficient for the scientific objective.

Table 1. Stylized excerpt of the Science Traceability Matrix (STM) including a reference orbital geometry highlighting the positions and times of the various observations, color-coded based on the specific Science Objectives (SO). The table includes the physical quantities that will be observed and derived to answer the Science Questions (SQ), as well as the list of instruments used for the observations. The footnotes at the bottom specify the necessary quantity ranges and accuracies required for the respective observations.

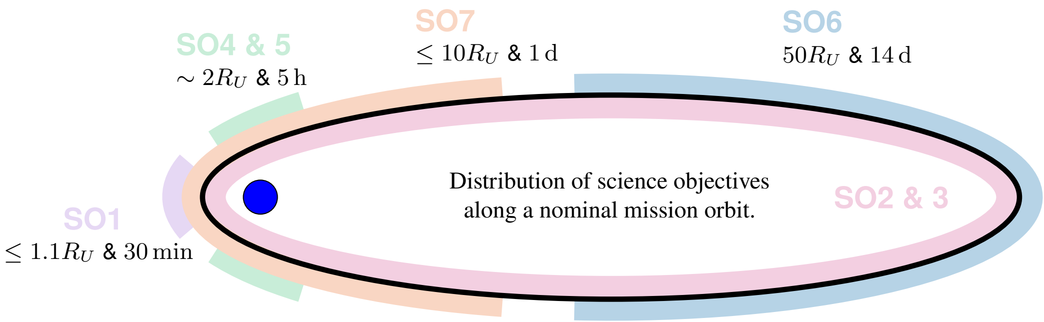

Scientific Question	Science Objective	Magnetic Field Strength	Gravity Potential	Plasma Density	Plasma Temp/Energy	Plasma Bulk Velocity	Plasma Composition	Plasma Energy Spectra	Turbulence Frequency	Auroral Brightness	Electron Flux	Chorus Wave Intensity	Chorus Wave Frequency	Electric Field Spectra	Electron Flux Pitch Angle	Priority	Instruments
SQ1. What governs the global structure and variability of Uranus's magnetosphere?	**SO1.** Determine the processes controlling the structure and variability of Uranus's magnetosphere.	•[1]	•[8]													1	MAG, Radio Sci. + USO
SQ2. How is energy transferred from the solar wind into Uranus's magnetosphere?	**SO2.** Determine the occurrence and frequency of magnetic reconnection at Uranus's magnetopause.	•[2]		•[5]	•[9]	•[12]		•[15]	•[16]							2	MAG, RPWI, JDC
	SO3. Determine the governing processes responsible for energy transfer between the solar wind and the magnetosphere, and quantify their efficiency.	•[2]														2	MAG[2]
SQ3. What controls Uranus's auroral emissions and how do they interact with the atmosphere?	**SO4.** Determine how auroral location, brightness, and morphology vary with Uranus's rotating magnetic geometry.	•[3]								•[17]						3	MAG[3], UV Camera
	SO5. Determine the precipitating particles producing Uranus's auroras and determine their effect on the atmosphere.				•[18]						•[19]					3	JDC
SQ4. How does Uranus lose atmospheric plasma to space?	**SO6.** Determine the geometrical structure of plasmoids in the magnetotail and estimate their contribution to atmospheric ion loss.	•[4]		•[6]	•[10]	•[13]										4	MAG, RPWI
SQ5. Does CIR-driven seed particle injection and local wave–particle acceleration, rather than internal plasma production, sustain Uranus's anomalously intense electron radiation belts?	**SO7.** Determine whether lower-band chorus-wave acceleration is the dominant mechanism driving Uranus's intense radiation belts, and whether magnetospheric pre-conditioning enhances the efficiency of CIR-driven acceleration.	•[1]		•[7]								•[20]	•[21]	•[22]	•[23]	5	MAG, RPWI, JoEE
	SO8. Determine the dynamics of energetic particles within Uranus's radiation belts.				•[11]		•[14]									5	JDC, JoEE

Individual science requirements:

[1] [0.1, 20000] nT, $< 1\%$
[2] [1, 30] nT, $< 1\%$
[3] [1, 2875] nT, $< 1\%$
[4] [0.1, 10] nT, < 0.1 nT
[5] [0.01, 0.1] cm^{-3} $<20\%$
[6] [0.001, 1] cm^{-3} < 0.0001 cm^{-3}
[7] $[10, 5 \cdot 10^7]$ $cm^{-2}s^{-1}$ sr^{-1} $< 20\%$
[8] Doppler shift: 0.01 mm/s
[9] [1,10000] eV $< 25\%$
[10] [10, 140] & [140, 5950] eV $< 25\%$
[11] [3, 200] keV/nuc $< 25\%$
[12] <500 km/s $< 15\%$
[13] [100, 7000] km/s <10 km/s
[14] [1 to 16] amu^{-1} $< 10\%$
[15] [1,10000] eV $< 25\%$
[16] [3, 400] Hz $< 10\%$
[17] 100-120nm, [0.05 to 30] kR $< 20\%$
[18] [30, 0000] eV $< 25\%$
[19] $[10^1, 5 \cdot 10^7]$ $cm^2s^{-1}sr^{-1}$ $< 20\%$
[20] $[3 \cdot 10^{-11}, 10^1]$ nT^2Hz^{-1} $< 20\%$
[21] [1400,7000] Hz with $< 5\%$
[22] $[3 \cdot 10^{-17}, 10^{-6}]$ $V^2 m^{-2} Hz^{-1}$ $< 20\%$
[23] $[0,180]^{circ}$ $< 15\%$

4. INSTRUMENTATION

4.1. Magnetometer

The proposed magnetic field investigation is derived from the JUICE J-MAG instrument (Brown et al., 2024), scaled to meet the mission-specific mass constraints. The measurement suite consists of two tri-axial fluxgate magnetometers and one scalar magnetometer based on the Zeeman effect.

To mitigate spacecraft-generated electromagnetic interference while adhering to strict weight limits, the sensors are accommodated on a shortened 7-meter deployable boom made of non-magnetic materials. To further isolate noise and protect sensitive components, the instrument's Data Processing Unit and supporting electronics are housed inside the main spacecraft bus.

The dual fluxgate gradiometric configuration allows the continuous characterization and subtraction of the dynamic magnetic field generated by the spacecraft itself. Concurrently, the scalar sensor provides an absolute magnetic field reference, which enables continuous, closed-loop in-flight calibration of the sensors to maintain ultra-high accuracy which is required in order to derive the magnetic and the inference of the acceleration by the chorus-wave based on the measurements of the magnetic strength.

Table 2. Magnetometer specifications.

Quantity	Measurement Range	Resolution
Magnetic Field Strength	$0.1 - 20000$ nT	± 0.002 nT

4.2. Radio Science + USO

The gravity experiment will make use of a Radio Science and Ultra Stable Oscillator USO (Tortora et al., 2023), with stations on Earth and an onboard accelerometer measuring only non-gravitational forces and sending this back as standard telemetry.

The Earth stations will measure the spacecraft's total acceleration using the Doppler shift of a reflected radio signal (from the spacecraft). Subtracting the accelerometer data from the total acceleration reveals the planet's gravity field. This allows for insight in its internal structure.

4.3. Particle Package

The particle package that will be utilized in this mission is derived from the JUICE specialized particle detection sensors which represents parts of JUICE's broader PEP (Particle Environment Package) (Barabash et al., 2023).

JoEE (Jovian Energetic Electrons) This low energy electron and ion spectrometer makes use of an electric field to filter incoming ions by their energy, and then measures their exact time of flight between detectors to calculate their mass and composition. This allows to determine the exact composition and dynamics of the surrounding plasma.

JDC (Jovian Dynamics and Composition) A spectrometer for higher energy electrons that relies on 3D printed collimators that act like directional channels, obtaining electron spectra almost simultaneously from nine different directions (Wittmann, 2022).

Table 3. Particle Package specifications.

JoEE Quantity	**Measurement Range**	**Accuracy**
Electron Energy	25 keV $-$ 1 MeV	$\pm 20\%$
Field of View	$12^\circ \times 180^\circ$	$\pm 12^\circ \times 22^\circ$
JDC Quantity	**Measurement Range**	**Accuracy**
Plasma Energy	1 eV $-$ 41 keV	$\pm 12\%$
Mass of a Partile	$1 - 70$ u	$\pm 4\%$

4.4. RPWI

For the radio and plasma wave investigation, we propose an instrument suite derived from the JUICE RPWI (Wahlund et al., 2024). It consists of three primary components: a Search Coil Magnetometer to measure high-frequency magnetic field fluctuations, a Radio Wave Instrument to measure the electric field vector and four Langmuir Probes that measure current-voltage characteristics to derive local plasma properties. By combining field data, the electromagnetic wave power spectral density is computable.

The RPWI sensors require specific spatial accommodation to avoid electrostatic and electromagnetic interference from the spacecraft bus. The SCM is co-located on the deployable MAG boom, while the RWI antennas and Langmuir probes are mounted on dedicated rigid booms extended from the main body to ensure an adequate spatial baseline.

Table 4. RPWI specifications.

Quantity	Measurement Range	Accuracy
Plasma Density	$10^{-5} - 10^{4}$ cm^{-3}	$\pm 5\%$
Electric Field Spectrum	$0 - 1.6$ MHz	$\pm 2 \frac{\mu V}{m\sqrt{Hz}}$
Magnetic Field Spectrum	0.1 Hz - 20 kHz	$\pm 8 \frac{pT}{\sqrt{Hz}}$

4.5. UV Camera

The proposed UV camera is a custom-designed, 2D photon-counting imager with a $10^\circ \times 10^\circ$ field of view. It is designed to achieve a spatial resolution of approximately 50 km and a SNR ratio of about 10 for a 1 kR auroral emission with an exposure time of 0.7s. Although the exact instrument must still be designed, the concept has a strong heritage. It relies on technologies demonstrated by Swift-UVOT (Roming et al., 2004), particularly its MCP-intensified detector readout and filter-wheel operation.

Table 5. UV Camera specifications.

Quantity	**Measurement Range [nm]**
Science Channels	$100-120$, $120.5-122.5$, $155-165$
Background Correction	$180-195$

4.6. Visible Light Camera

The inclusion of the visible light camera is primarily for outreach. Based on the JunoCam (Hansen et al., 2017), it will take the first images of Uranus since Voyager II (1986), as well as having the possibility to take images of Venus during the gravity assist.
It operates as a push-frame imager with Time-Delay Integration (TDI) serving as an economic option to take rapid frame strips.

5. MISSION DESIGN

5.1. Earth-Uranus Transfer

The UMEO mission adopts an interplanetary transfer from Earth to Uranus using a Multiple Gravity Assist (MGA) trajectory to reduce the launch energy required and remain compatible with current European launch capabilities. The baseline scenario targets a launch on 8 January 2038 based on opportunities from a past mission concept (Amy et al., 2023) with a time of flight of 14.2 years, allowing arrival during the early 2050s, while an alternative launch opportunity in 2045 has been investigated as a backup scenario based on long-term trajectory studies (Mudek, 2022). Following a trade-off between available launch vehicles, Ariane 64 was selected as the baseline launcher. Its payload capability of $2240\,\mathrm{kg}$ for the required launch energy (C3 = $35.5\,\mathrm{km^2/s^2}$) provides the best compromise between performance, availability and mission cost while remaining compatible with the spacecraft wet mass. The selected interplanetary transfer is illustrated in Figure 1. By using one Venus and two Earth flybys, the sequence of gravity assists reduces the launch energy required to reach Uranus while remaining compatible with the Ariane 64 launcher. After the interplanetary cruise, the spacecraft performs a Uranus Orbit Insertion (UOI) manoeuvre to achieve a highly elliptical orbit, with a maximum insertion mass of $990\,\mathrm{kg}$ into Uranus orbit, as given in Table 6. The propulsion budget is dominated by the UOI burn, with additional propellant allocated for orbit maintenance for up to 10 years and a controlled end-of-life disposal. A detailed Δv budget can be found in Table 7.

Table 6. Mass budget

Description	Mass (kg)
UMEO dry mass	849
Maximal dry mass	990
Propellant mass	1140
Total wet mass	2130

Table 7. Δv budget

Manoeuvre	Δv $(\mathrm{km\,s^{-1}})$
Uranus Orbit Insertion	1.87
Stationkeeping	0.15
End-of-Life	0.028
Total (inc. $10\,\%$ **margin)**	2.05

5.2. Science Orbit

The science orbit has been designed to maximize the mission's scientific return while satisfying operational and propulsion constraints. A highly elliptical and inclined orbit was selected to provide comprehensive coverage of Uranus' magnetosphere, enabling in-situ measurements at low altitude and global observations at large distances. This orbital configuration supports the mission's primary objectives, including the characterization of the planetary magnetic field, the investigation of auroral processes and the study of solar wind interactions with the Uranian magnetosphere and the provoked mass loss event.
The nominal science orbit is characterized by a periapsis radius of 1.1 R_U, an apoapsis radius of 50 R_U (see the figure in Table 1 for the scientific reasoning of this orbit), and an inclination of 81° with respect to the Uranian equator. The orbital plane is close to the ecliptic plane, enabling repeated observations of the magnetic poles while minimising Δv cost for science orbit insertion. The 5-year nominal mission lifetime allows for 114

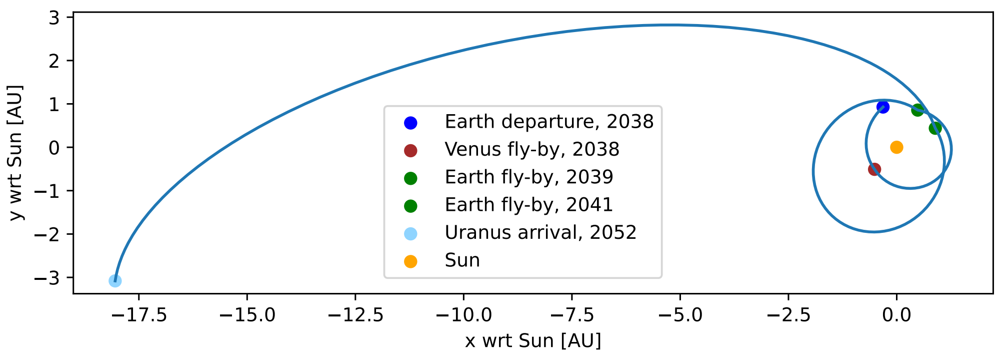

Figure 1. Baseline Earth-to-Uranus trajectory using an EVEEU gravity assist sequence obtained with the TUDAT library (Dumont et al., 2022). Total time of flight is 14.2 years.

revolutions around the planet. Orbital parameters are summarised in Table 8.

Table 8. Nominal science orbit parameters.

Orbital Parameter	Value	Unit
Periapsis radius	1.1	R_U
Apoapsis radius	50.0	R_U
Inclination	81.0	°
Eccentricity	0.957	-
Orbital period	16.0	d

In accordance with the COSPAR Planetary Protection Policy (Committee on Space Research, 2026), the spacecraft will perform a controlled disposal manoeuvre at the end of the mission. After completing its scientific objectives and no extended mission programm, the spacecraft will perform a retrograde burn at apoapsis to lower periapsis and ensure atmospheric entry into Uranus, preventing any long-term orbital evolution that could lead to an accidental impact with one of the planet's natural satellites. This disposal strategy minimizes the risk of forward contamination of potentially significant icy moons and complies with international planetary protection recommendations (Committee on Space Research, 2026).

6. SPACECRAFT ENGINEERING

Sending a spacecraft to Uranus represents a technically challenging endeavor that requires extensive analysis and robust system design. The mission demands high radiation tolerance, precise thermal control, the use of radioisotope thermoelectric generators and reliable long-distance communication capabilities. The main mass constraint is imposed by the selection of the Ariane 64 launch vehicle.

6.1. Spacecraft Design

6.1.1 Propulsion and AOCS

The spacecraft relies on an R-4D 490 N bipropellant main engine with a specific impulse of 315.5 s to execute major maneuvers, including the critical Uranus Orbit Insertion. The MMH/MON-3 propellants are delivered via a pressure-fed system using helium stored at 31 MPa, regulated to an operating pressure of 20 bar. Additionally, precise three-axis attitude control and momentum wheel desaturations are managed by sixteen 4 N thrusters.

6.1.2 Mass Budget

Table 9. Mass budget overview listing the estimated masses for the individual systems and including a system-based margin as well as a total system margin.

System	**Mass** (kg)	**Margin** (%)	Total (kg)
Structure	170.6	20	173.1
Thermal	32.0	10 to 20	36.2
Payloads	68.5	10 to 20	79.9
Power	81.3	10 to 20	91.9
C&DH	32.1	10 to 20	38.5
Communication	49.9	20	71.3
AOCS	20.9	10 to 20	44.9
Propulsion	156.1	10	171.7
Sum			707.5
w/ platform margin		20	849.0

Table 9 presents an overview of the estimated masses of the entire spacecraft, distributed over its various systems. Each system's mass has been conservatively estimated, and another system margin has been applied to it. Finally, a total platform margin of 20 % has been added to the mass sum over all systems. The final value

6.1.3 Power Budget

The spacecraft uses a GPHS-RTG as the primary power source, benefiting from extensive flight heritage from missions such as Galileo, Cassini-Huygens, and New Horizons. The initial power output of the RTG is approximately 300 W, decreasing to approximately 236 W at the EOL (30 years). As a secondary power source, the spacecraft uses LiFePO 4 batteries with a specific energy of 160 Wh/kg. These batteries were selected due to their tolerance to temperature and ionizing radiation and their long operational lifetime. The battery system has a beginning-of-life capacity of 2025 Wh. The duty cycles of individual spacecraft components will be determined during subsequent iterations of the spacecraft power budget.

Table 10. Power budget overview.

System/Instrument	**Power Consumption** (W)
Thermal	100.0
C&DH	19.2
AOCS	
Star tracker	7.9
Star tracker electronics	11.5
Reaction wheel	24.0
IMU (gyros + accel)	21.0
Coarse rate sensor	5.5
Comms	
Ka data downlink	60.0
X data downlink	60.0
Ka/X Receiver	15.0
Payload	
RPWI	21.8
JDC	8.0
JoEE	10.0
UV Camera	4.4
Radio	2.0
Magnetometer	6.0

Table 10 shows an overview of the maximum power consumption of the instruments and other subsystems used in this mission. Note that not all instruments, as well as the subsystems, require the indicated power the entire time, but only during specific and staggered periods.

6.1.4 Data Budget

The data budget (see Table 11) is based on a preliminary estimate of the data generated by each subsystem and the corresponding measurement duration during a single orbital period.

With an estimation of about 19.4 Gb of total data produced per orbit and with an approximate data downlink capability for ESA ESTRACK of 30 kbps (see Sec. 6.1.5 for additional information), every orbit shall include a downlink period up to 51.2 h.

Table 11. Data budget overview. Assuming factor 2 loss-free compression and 1 optical camera image per orbit.

Instrument	**Data per Orbit** (kb)
RPWI	9 925 269
JDC	254 448
JoEE	239 241
UV Camera	5 515 776
Magnetometer	220 579
Optical Camera	120 000
Sum	16 275 314
w/ compression	8 197 657

6.1.5 Link Budget

The link between the spacecraft and the ground station is established via a *Ka-band* link for data downlink (32 GHz) and an *X-band* link for telemetry and control (downlink at 8.4 GHz, uplink at 7.15 GHz). As ground stations, both ESA European Space Tracking (ESTRACK) and NASA Deep Space Network (DSN) antennas can be used. The NASA DSN 70 m ground station supports a downlink data rate of up to 88.1 kbps and an uplink data rate of up to 234 kbps. The ESA ESTRACK 35 m ground station supports a downlink data rate of up to 33.5 kbps and an uplink data rate of up to 783 kbps. The spacecraft antenna is a 2.5 m dish (the same diameter as the JUICE mission antenna) with a dish depth of 0.39 m and a focal length of 1 m, featuring two feeds at the vertex and a hyperboloidal subreflector. The estimated mass of this antenna is between 30 and 40 kg. The gain of this antenna is 56.24 dBi for the *Ka-band* and 44.63 dBi for the *X-band*. The modulation scheme used for all links is BPSK with low-density parity-check (LDPC) coding, with a code rate of 1/2 and a target BER of 10^{-6}. An additional 3 dB margin was added to the required E_b/N_0 to account for uncertainties in system performance. The communication subsystem uses two X/X/Ka-band transceivers, which were developed by Thales Alenia Space Italy for the BepiColombo mission and have a TRL of 9. One transceiver operates as a cold redundant unit. Each transceiver has two power conditioning units, one of which is operated in cold redundancy. Each transmitter can simultaneously transmit and receive on three channels (X-*TX*, X-*RX*, Ka-*TX*). The pointing accuracy required to maintain 90 % of the downlink data rate is $0.05°$ for *Ka-band* and $0.2°$ for *X-band*. The Ka-band downlink budget (Table 12) is evaluated for the maximum Earth-spacecraft distance of 20.05 AU, representing the worst-case communication scenario. A system noise temperature 35 K was assumed, corresponding to a high-performance Ka-band deep-space ground station under favorable operating conditions. The received carrier-to-noise density ratio was calculated from the received signal power and the assumed ground station system noise temperature. The required E_b/N_0 was assumed on the heritage of the BepiColombo mission, with a code rate of 1/2, which reduced the required E_b/N_0 for a target bit error rate (BER) of 1×10^{-6} to approximately 1 dB. Ionospheric losses for both Earth and Uranus were assumed to be negligible. Atmospheric losses were estimated for clear-sky conditions at zenith, assuming a tropospheric attenuation coefficient of 0.1 dB/km and a troposphere height of 12 km, resulting in a total tropospheric loss of 1.2 dB. This represents a best-case atmospheric attenuation assumption. The RF subsystem losses include waveguide losses, connector losses, and remaining implementation losses within the RF chain.

Table 12. Ka-band downlink budget overview.

Property	**Value**	**Unit**
Link distance	3×10^{12}	m
	20.05	AU
Frequency (Ka)	32	GHz
Wavelength	9.38	mm
3 dB beamwidth	0.2625	°
Spacecraft antenna gain	56.24	dBi
ESA ESTRACK gain	80.3	dBi
NASA DSN gain	84.5	dBi
TX output power	14.77	dBW
	30	W
Free space loss	312.09	dB
Tropospheric loss	1.2	dB
Pointing loss (0.05°)	0.44	dB
RF subsystem losses	1.08	dB
Required E_b/N_0	1	dB
E_b/N_0 margin	3	dB
Ground station T_{sys}	35	K
ESA ESTRACK 35 m		
Received signal power	−161.33	dBW
C/N_0	51.83	dBHz
LDPC coded data rate	60.62	kbps
Useful data rate	30.31	kbps
NASA DSN 70 m		
Received signal power	−157.13	dBW
C/N_0	56.03	dBHz
LDPC coded data rate	159.44	kbps
Useful data rate	79.72	kbps

6.1.6 Thermal Engineering

The thermal control is governed by the Worst Hot Case (WHC) and Worst Cold Case (WCC). The WHC occurs during the planned fly-by maneuver at Venus, where the solar irradiance will reach its peak around approx. $2000\,\mathrm{W\,m^{-2}}$. Additionally, the spacecraft will be exposed to IR thermal emission from Venus and albedo radiation reflected from Venus' surface. This additional heat load must be efficiently radiated away together with the dissipated heat from the RTGs. The WCC occurs near the end-of-mission (EOM) around Uranus' orbit at the apoapsis, where the solar flux will be minimal, paired with an almost negligible IR flux from Uranus' surface and already degraded and, thus, minimal dissipated heat flux from the RTGs.

These two cases drive the thermal design in two different ways. During the WHC, the spacecraft must efficiently radiate heat, which will be achieved by using a large radiator with a high-emissivity surface coating, constantly facing away from the Sun. During the WCC, the spacecraft must efficiently contain heat, necessitating high insulation efficiency, achieved through rigorous use of multi-layer insulation. Temperature control of our electronics compartment during and between these two extreme cases is provided by thermostatically controlled louver assemblies that provide an internal operating range near room temperature. The louvers rotate open when large amounts of heat are dissipated (during WHC).

6.2. Risk Analysis

A reliability block diagram (RBD) was created to define the single-chain high-level system functions required for mission success. By identifying failure modes for each high-level RBD function, a Failure Mode, Effects and Criticality Analysis (FMECA) was derived. The main risk drivers identified by the FMECA were categorized using a risk matrix, as shown in Table 13.

Key risks were mitigated through a late-mission orbit-lowering capability, a backup launch opportunity, and observation strategies using multiple spacecraft attitudes and additional instruments. A five-year lifetime was defined as the minimum success criterion, with propellant margin retained for an operational extension up to 15 years. Solar-conjunction outages of up to 17 days were identified and accommodated through sufficient science payload data storage and pre-planned safe mode operation‘.

Table 13. Main risk drivers matrix: Occurrence versus Severity. No catastrophic risk drivers were identified.

	Severity	
Occurrence	**High**	**Major**
High	Limited launch window	**Atmospheric drag**
	Limited instrument field of view and configuration	
Low	Cannot establish an Earth link or provide minimum pointing accuracy	
	Minimum acceptable mission duration of 6 years	
	Communications to Earth blocked by the Sun	
	Sufficient performance launcher unavailable	
	Uranus orbit cold case	
	Inactive instrumentation during transfer	

Table 14. Cost estimate.

Item	Cost [M€]	Percentage [%]
Spacecraft	650	47.7
Extra payload engineering	20	1.5
RTG	200	14.7
ESA management cost	168	12.3
Mission operations	90	47.7
Science operations	80	6.6
Launcher (Arianne 64)	135	9.9
Nuclear regulations	20	1.5
Total	**1363**	**100**

7. COST ESTIMATE

The total mission cost is estimated at 1363 M€. The vast majority of the budget is allocated to the spacecraft segment, which includes industrial costs, RTG integration, and full mission and science operations. The remainder covers the launch via Ariane 64 and necessary nuclear regulations.

8. DE-SCOPING OPPORTUNITITES

Should de-scoping be required, instruments will be removed in reverse order of their mission priority (see subscript of Table 1), beginning with the lowest-priority objectives and preserving the core mission requirements for as long as possible:

1. Visible Light Camera, as its objectives are secondary and non-essential to the mission.
2. JoEE, as the only objectives it addresses (SO7 and SO8) are of lower priority
3. UV Camera, for similar reasoning regarding SO4
4. JDC and RPWI, for similar reasoning regarding objectives SO2, SO3,SO5, SO6, SO7, SO8
5. Radio Science + USO and Magnetometer, as these fulfil the primary mission objectives and are therefore of the highest priority

By incrementally de-scoping the mission we can reduce the total dry mass, potentially unlocking new launch opportunities, and driving down total mission cost.

9. CONCLUSION

The UMEO mission will aim to investigate Uranus's unique and poorly understood environment. Through long-term measurements of its magnetic and gravitational field, plasma environment and radiation belts, UMEO will address fundamental questions about magnetospheric dynamics and the interaction with the solar environment. It will also strengthen the connection between Solar System exploration and exoplanet research, since Uranus represents one of the closest analogues to the most abundant population of exoplanets. Overall, at least 5 years of science will provide a new foundation for understanding how high energy processes affect planetary structure and evolution.

References

Allen, R. C. et al. (2025). *GRL* 52.
Amy, S. et al. (2023). Mission Concept Study. NASA.
Barabash, S. et al. (2023). Vol. 55. AAS/Division for Planetary Sciences Meeting Abstracts.
Bhardwaj, A. et al. (2000). *Reviews of Geophysics* 38.3.
Brown, P. et al. (2024). *EGU General Assembly 2024*, EGU24-1750.
Committee on Space Research (2026). *Space Research Today* 224.
Connerney, J. E. P. et al. (1987). *JGR: Space Physics* 92.A13.
DiBraccio, G. A. et al. (2019). *GRL* 46.19.
Dumont, J. P. et al. (2022). *Europlanet Science Congress 2022*.
Fletcher, L. et al. (2020). *PSS* 191.
Gronoff, G. et al. (2020). *JGR: Space Physics* 125.8.
Hansen, C. J. et al. (2017). *SSR* 213.1.
Herbert, F. (2009). *JGR: Space Physics* 114.A11.
Jasinski, J. M. et al. (2024). *Nature Astronomy*.
Joshi, S. et al. (2025). *A& A* 693.

Lamy, L. (2020). *Philosophical Transactions of the Royal Society of London Series A* 378.2187, 20190481.
Lamy, L. et al. (2012). *GRL* 39.7.
Liu, D. et al. (2026). *arXiv:2601.03659*.
Ma, X. et al. (2017). *JGR: Space Physics* 122.10.
Masters, A. (2014). *JGR: Space Physics* 119.7.
Mauk, B. H. et al. (2010). *JGR: Space Physics* 115.A12.
McNutt Jr., R. L. et al. (1987). *JGR: Space Physics* 92.A5.
Melin, H. et al. (2025). *GRL* 52.22.
Millholland, S. et al. (2019). *Nature Astronomy* 3.
Mudek, A. J. (2022). Ph.D. dissertation. Purdue University.
Parisi, M. et al. (2024). *PSJ* 5.5.
Paty, C. et al. (2020). *Philosophical Transactions of the Royal Society of London Series A* 378.2187.
Richardson, J. et al. (1988). *GRL* 15.8.
Roming, P. W. A. et al. (2004). Vol. 727. AIP.
Sibeck, D. G. et al. (2022). *JGR: Space Physics* 127.9, e30704.
Simon, A. et al. (2021). Tech. rep. NASA/TP-2021000000. NASA & JHU/APL.
Stanley, S. et al. (2004). *Nature* 428.6979.
Stone, E. C. et al. (1986). eng. *Science (AAAs)* 233.4759.
Tortora, P. et al. (2023). Vol. 2808. LPI Contributions.
Treumann, R. A. et al. (2001). Dordrecht: Springer Netherlands.
Turner, D. L. et al. (2024). *JGR: Space Physics* 129.8.
Wahlund, J.-E. et al. (2024). *SSR* 221.1.
Wittmann, P. (2022). PhD thesis. Umeå University.